AJNR

Aberrant Diffusion and Geometric Properties in the Left Arcuate Fasciculus of Developmentally Delayed Children: A Diffusion Tensor Imaging Study

J.-W. Jeong, S.K. Sundaram, A. Kumar, D.C. Chugani and H.T. Chugani

ORIGINAL RESEARCH

J.-W. Jeong
S.K. Sundaram
A. Kumar
D.C. Chugani
H.T. Chugani

🔓

Aberrant Diffusion and Geometric Properties in the Left Arcuate Fasciculus of Developmentally Delayed Children: A Diffusion Tensor Imaging Study

BACKGROUND AND PURPOSE: One of the neurologic substrates of poor language in children with DD is the abnormal development of perisylvian language networks. We sought to determine whether this manifests as aberrant regional changes in diffusivity or geometry of the left AF.

MATERIALS AND METHODS: We performed DTI studies in 16 young (age, 55.4 ± 18.95 months) patients with DD and 11 age- and sex-matched TD children (age, 60.09 ± 21.27 months). All children were right-handed. To detect the malformation of left AF structure in native or standard space, we proposed new methodology consisting of 2 complementary approaches, principal fiber orientation quantification in color-coded anisotropic maps and tract-based morphometry analysis.

RESULTS: Patients with DD did not show the typical pattern of age-related maturity of the AP and ML pathways passing through the left AF (R^2 of the AP pathway: DD versus TD = 0.002 versus 0.4542; R^2 of the ML pathway: DD versus TD = 0.002 versus 0.4154). In addition, the patients with DD showed significantly reduced FA in the temporal portion of the AF (mean FA of DD versus TD = 0.37 ± 0.11 versus 0.48 ± 0.06, $P <$ .001), and the AF showed higher curvatures in the parietotemporal junction, resulting in sharper bends to the Wernicke area (mean curvature of DD versus TD = 0.12 ± 0.03 versus 0.06 ± 0.02, $P <$ .001).

CONCLUSIONS: The proposed methods successfully revealed regional abnormalities in the axonal integrity of the left AF in the patients with DD. These abnormalities support the notion that the perisylvian language network is malformed in children with DD.

ABBREVIATIONS: AD = axial diffusivity; AF = arcuate fasciculus; AP = anteroposterior; CA = color-encoded anisotropy; DD = developmental delay; DTI = diffusion tensor imaging; FA= fractional anisotropy; FDR = false discovery rate; GM = gray matter; H = hypothesis; MD = mean diffusivity; ML = mediolateral; MNI = Montreal Neurological Institute; RD = radial diffusivity; s = arc-length coordinate; SPM = Statistical Parametric Mapping; SPM-DARTEL = Statistical Parametric Mapping Diffeomorphic Anatomical Registration Through Exponentiated Lie Algebra; TBM = tract-based morphometry; TD = typically developing; VBM = voxel-based morphometry; WM = white matter

Global DD in children is characterized by significantly delayed development in ≥2 of the following developmental domains: gross/fine motor, speech/language, cognition, social/personal skills, and activities of daily living. In particular, this is almost always accompanied by significant delay in the development of speech/language. While the neurologic substrate of normal speech development involves the perisylvian language networks in the left cerebral hemisphere and has been studied for more than a century, to our knowledge, the neurologic basis of speech delay has not been widely studied. An earlier preliminary DTI study on patients with DD found

that these patients showed abnormal diffusivity changes in the centrum semiovale, corona radiata, internal capsule, corpus callosum, and subcortical WM of the frontal and parieto-occipital lobes.[1] In a recent study of children with DD, by using DTI we found that the major language tract in the left (dominant) hemisphere (ie, the AF) could not be identified in a significant proportion of the children.[2] This finding was even more dramatic in Angelman syndrome, a severe developmental disorder with cognitive delay, epilepsy, and virtually absent speech, because the AF could not be identified in almost every child with the disorder.[3]

This finding suggests that aberrant development of the AF region is a key factor in delayed speech development. Moreover, the neuroradiologist who interprets the standard clinical structural MR imaging scan by visual analysis (without DTI) is unable to detect such abnormalities. While our prior studies established that the AF is abnormally formed or unidentifiable in children with DD and Angelman syndrome, these studies did not adequately characterize the abnormality along the whole length of the AF. Although our studies could not identify the AF in a significant number of these children, we did not investigate the impact of regional variations in DTI parame-

ters along the AF pathway on the identifiability of the AF in these children.

Normal development of white matter tracts is dependent on regional concentration gradients of axon-guidance molecules, a process that is under genetic control.[4] Thus, any functionally significant mutations/polymorphisms in axon guidance pathways could result in regionally disorganized WM bundles (with abnormal DTI parameters, such as low FA, abnormal shape or curvature, and so forth), which could manifest as unidentifiable/malformed tracts. The present study was designed to determine whether regional variations in DTI parameters along the AF bundle exist in children with DD. We took 2 complementary approaches: 1) a region-of-interest analysis for fiber-orientation distribution that quantifies the regional distribution of the left AF directionality, and 2) TBM analysis of the left AF, which quantifies local variation in the shape of this tract along its whole length. Most important, this type of analysis allows one to evaluate the whole group of patients with DD whether the tract is identifiable or not. In addition, this analysis could demonstrate the regional abnormalities along the course of the AF that resulted in the unidentifiability of the AF in our prior study.[2]

TBM analysis has been applied to investigate subtle alterations in diffusion parameters of the AF and cingulum.[5] This method spatially normalizes the fibers of multiple subjects in standard space and then registers the coordinates of individual fibers to those of a group-standard fiber, followed by statistical analysis of DTI parameters only at the common coordinates of group subjects. Unlike other VBM analyses such as tract-based spatial statistics[6] (www.fmrib.ox.ac.uk/fsl/tbss) and tissue-specific smoothing-compensated voxel-based analysis,[7] this analysis uses the WM trajectory for the between-subject registration, thus enabling the user to assess shape features (curvature) in the direction of the entire fiber bundle. We believe that the use of fiber trajectories to register the values of DTI parameters across subjects will probably yield less registration error, which highly depends on the differences in individual morphology and will be more suitable for performing multiple comparisons for group analyses because the parameter values are directly sampled at anatomically equivalent locations.

Materials and Methods

Subjects

Sixteen children with the diagnosis of DD (age, 55.4 ± 18.95 months; 9 males) and 11 TD children (age, 60.09 ± 21.27 months; 9 males) underwent DTI and developmental-behavioral assessments. Four of the patients with DD were part of our previous study, and the AF was unidentifiable in these 4 patients.[2] All patients had been referred to the Children's Hospital of Michigan Neurology Clinic. The diagnosis of DD was made by an experienced pediatric neurologist. Patients with the following conditions were excluded from the study: history of seizures, history of prematurity or a perinatal hypoxic-ischemic event, focal deficits on clinical examination by a pediatric neurologist, dysmorphic features suggestive of a clinical syndrome, structural clinical MR imaging interpreted as abnormal by a pediatric neuroradiologist, positive findings on cytogenetic and/or fragile X tests, or the presence of an inborn error of metabolism.

All children in the study were right-handed. The group did not differ as to age ($P = .28$) or sex ($P = .5$). Written and informed consent was obtained from 1 of the parents or legal guardians of the TD participants. The Human Investigations Committee at Wayne State University granted permission for the retrieval and analysis of the clinical data and MR imaging scans of children with DD.

Data Acquisition and Preparation

All DTI scans were obtained on a 3T Signa scanner (GE Healthcare, Milwaukee, Wisconsin) equipped with an 8-channel head coil at TR = 1250 ms, TI = 88.7 ms, FOV = 240 cm, 128 × 128 acquisition matrix, contiguous 3-mm-thick sections to cover all the axial sections of the whole brain by using 6 isotropic gradient directions with $b = 1000$ s/mm^2, 1 $b = 0$ acquisition, and NEX = 6 to increase the signal intensity–to-noise ratio and to reduce the artifacts. Approximate scanning time for the DTI acquisition was 9 minutes by using a double refocusing pulse sequence to reduce eddy current artifacts. An array spatial sensitivity encoding technique was also applied to further reduce the geometric distortion due to the sequence design.

To secure uniform quality of DTI data across the subjects, we corrected the $b = 1000$ s/mm^2 images for eddy current distortion and any potential movement during the DTI acquisition. We used the Functional MR Imaging of the Brain Software Library module for this correction (Oxford Centre for Functional Magnetic Resonance Imaging of the Brain Software Library; http://www.fmrib.ox.ac.uk/fsl/fdt). The correction relies on a 12-parameter affine transformation.

Data Analysis

This study presents sequential modules to identify significant variations of DTI features between the TD and DD groups. These variations were systematically assessed in 2 distinct spaces: the subject's native head space (x,y,z) and standard MNI space (u,v,w). The methodology was implemented by the following 4 modules.

Estimation of DTI Parameters

Spatial maps of diffusion tensors at every voxel of native space were evaluated by using an in-house–implemented software incorporating a signal intensity–to-noise-ratio-weighed multivariate least squares fitting approach.[7] On the basis of the first eigenvector (v_1) and 3 eigenvalues ($\lambda_1,\lambda_2,\lambda_3$) of the diffusion tensor matrix, we reconstructed diffusion parameter maps, including FA [3 × variance of ($\lambda_1,\lambda_2,\lambda_3$) / ($\lambda_1{}^2+\lambda_2{}^2+\lambda_3{}^2$)]$^{1/2}$, a CA map [scaled-($v_{1x},v_{1y},v_{1z}$)], MD [($\lambda_1+\lambda_2+\lambda_3$) / 3], AD (AD = λ_1), and RD [($\lambda_2+\lambda_3$) / 2] at every voxel of native space.[8,9] The Frenet equation[10] was applied to measure the scale-free fiber curvature—that is, for a given fiber, its curvature was measured by the absolute magnitude of the first derivative of the tangent vector at the individual spatial coordinate.

Spatial Normalization of B0 image by Using SPM-DARTEL

To enable group analysis of DTI parameters across the subjects, we first aligned DTI parameter maps of individual subjects in standard space via a nonlinear deformation field that spatially normalized a B0 image of the individual subject to a pediatric MNI B0 template. For this alignment, we used the SPM-DARTEL approach.[11,12]

For a given i^{th} subject, SPM-DARTEL iteratively seeks the deformation field, $M_i(x,y,z)$ that relates 1 voxel of native head space (x,y,z) to its corresponding voxel of the MNI space (u,v,w) with minimum mean square error. To estimate optimal $M_i(x,y,z)$, we first segmented tissue probability maps (ie, GM and WM) from the B0 image by using an SPM segmentation module. Then each tissue map was iteratively aligned and deformed to the corresponding map of the most repre-
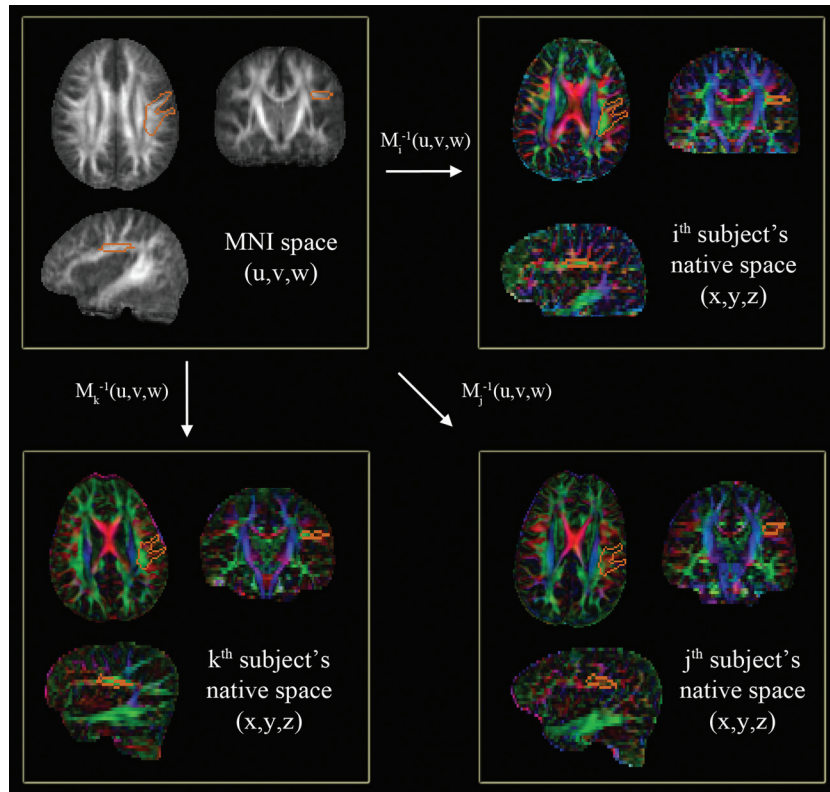
Fig 1. Automatic quantification of a CA map in the left AF region of native space. A single region of interest to enclose core voxels of the left AF (orange contour of the top left panel) is manually delineated on the MNI FA template (gray-scaled image in the top left panel). This region of interest is then transferred to individual CA maps (colored images) via the corresponding $M_i^{-1}(x,y,z)$. At each transferred region of interest, the sum of AP (green) and ML (red) components are calculated and compared across the subjects to quantify the degree of WM development in the left AF.

sentative TD subject, resulting in a nonlinear field to register the voxels of native space to those of the TD population space. The $M_i(x,y,z)$ is finally determined by a composite of the nonlinear field and an affine transformation between the GM coordinates of the TD space and those of the pediatric MNI space.[13] We repeated the above procedure to obtain the $M_i(x,y,z)$ for all subjects in both groups. Resulting $M_i(x,y,z)$ and its inverse, $M_i^{-1}(x,y,z)$ were directly applied to define spatial transformation of DTI parameter maps, whole-brain tractography, and regions of interest between the MNI space and native subject space.

Region-Based Quantification Analysis

The direction of individual fibers in DTI data can be imaged by CA maps,[14] in which 3 components of the eigenvector v_1 in association with the largest eigenvalue λ_1 are color-coded by using an RGB-color model, which is symmetric with respect to all color axes. The color axes are aligned with the patient coordinate system (green, AP; red, =ML; blue, SI). As a direct metric to quantify a measure of directional fiber volume in the AF fibers, we summed up AP components (v_{1y}, green component of the color-coded map) and ML components (v_{1x}, red component of the color-coded map) at the CA voxels of the AF region.

The quantification of the directionality at a specific region for the group comparison can be achieved by 2 different methods: 1) to manually delineate the same region of interest on the CA map that was acquired in subject's native space,[2,15] and 2) to normalize the tensor data of each subject to those of the MNI template space, reorient the tensor field according to the local transformation matrix, and calcu-

late the MNI-CA map from reoriented tensors.[16-18] The first approach is performed in the subject's native space, which is straightforward, but its reproducibility is limited.[19] It requires reproducible protocols and operator experience to secure inter-rater variability. The second approach is studied in template space, which is more efficient to evaluate a large amount of data in a systematic manner but adds uncertainty in the analysis because it needs nonlinear warping of the tensor field and artificial manipulation of the tensor measurement.[16,20] More important, it typically requires a time-consuming computational process to achieve reasonable accuracy in tensor normalization.[18]

Figure 1 shows a hybrid approach that represents a compromise of the above 2 approaches. It defines a transaxial region of interest in the left AF region in the MNI space (orange contours of the top left panel of Fig 1). This region of interest is manually delineated on the MNI FA map (gray-scaled images) and then transformed via the $M_i^{-1}(x,y,z)$ to the individual subject's head space (color maps). The inversely normalized region of interest (orange contours on each color map) is overlapped on the subject's CA maps to assess the total number of AP and ML components in the left AF region.

Because the $M_i^{-1}(x,y,z)$ allows a free deformation to match the regions of template space to those of the ith subject's space, the size and location of the normalized region of interest can be extended or contracted depending on the size and structure of the ith subject's brain. Thus, the total number of AP and ML components inside the normalized region of interest provides a direct measure of the AF fiber connection existing in AP and ML directions, which do not depend on any experimental variability. We evaluated this metric for all sub-
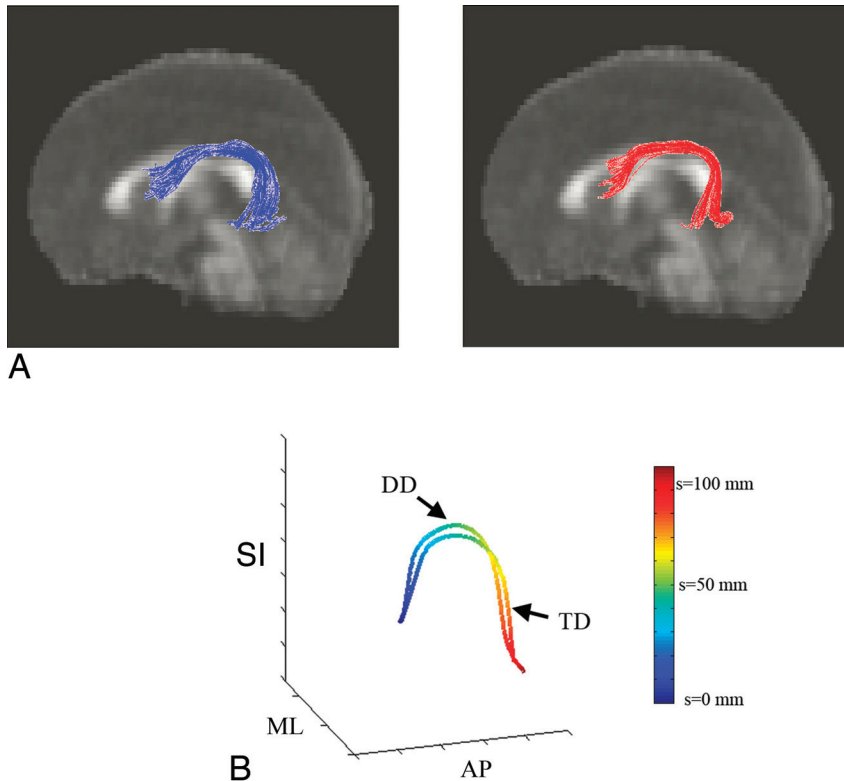
Fig 2. Preparation of TBM analysis. *A,* Input multisubject fiber bundles of the AF: left TD (blue) and right DD (red). *B,* Prototype fibers obtained from the TD and DD bundles and their arc-length parameterization. Two-millimeter arc-length coordinates along each prototype are blue (s = 0 mm) to red (s = 120 mm). Note that we define starting (blue)/ending (red) at the AP region for the left AF. According to this convention, we rearranged starting/ending points of all fibers in the bundle to match the starting/ending point of an arbitrary fiber to those of the prototype.

jects in both TD and DD groups. A 2-sample *t* test with equal variance corrected for multiple comparisons was used to examine the group difference.

TBM Analysis

The TBM analysis was recently reported to provide a new way to observe the local transition of DTI parameters along bilateral AF fibers of healthy adults,[5] where subtle differences of major eigenvalues existing in left and right AF fibers were clearly detected. This could not be found by conventional full-path analysis (ie, averaging of the parameter values existing in entire tracts). This analysis registers an individual subject's AF fibers to a standard fiber called a "prototype." The coordinates of individual fibers are spatially matched to corresponding coordinates of prototypes called "common arc-length coordinates." At each arc-length coordinate, the DTI parameter is calculated in each subject and the group difference is examined.

To construct left AF group fibers for the TBM analysis, we conducted whole-brain tractography per subject of each group by using conventional streamline tractography based on the Runge-Kutta order 2 interpolation at FA > 0.20, angular deflection < 60°, and step size = 0.2 mm. The coordinates of the resulting tracts were transformed to the MNI space via $M_i(x,y,z)$ to be registered across subjects. Two binary regions of interest (inferior frontal and middle temporal) of the anatomical automatic labeling map[21] (www.cyceron.fr/web/aal) were applied to isolate the left AF fiber bundle of each group.

To assure the consistency of individual fibers in the AF group bundle, we computed a group consistency map by summing up the number of fibers penetrating individual voxels in standard space. The voxels that the fibers passed through in at least half of the subjects of

each group were assumed to represent a "consistent pathway." The fibers existing inside the consistent pathway were subsequently considered for the analysis. The longest fiber penetrating the highest attenuation region in the TD group was selected as the prototype. Figure 2*A* shows the group bundle of the left AF obtained from both groups. The prototype of each group bundle is shown in Fig 2*B*. The common arc-length coordinates for each group were placed every 2-mm arc-length along each prototype as color-coded in Fig 2*B*.

In this study, we used the arc-length coordinates of the TD prototype for the group comparison—that is, at each arc-length coordinate of the TD prototype, its corresponding coordinate of individual fiber in both groups was identified by an optimal point-match method based on the Hungarian matching algorithm.[5] The parameter values of both groups at these matched coordinates were pooled together and then examined by a 2-sample *t* test under 2 different contrasts (TD > DD and TD < DD), which were controlled for age. The FDR *P* value[22] was considered for multiple comparisons. Variations in diffusion parameters (FA, MD, AD, and RD) and the geometric parameter (curvature) were examined along all arc-length coordinates (FDR-corrected *P* value > .05).

Results

Region-Based Quantification Analysis

Figure 3 presents the results of region-based quantification of the AP (green) component and the ML (red) component in the CA map, plotted against the subject's age in the TD and DD groups. There is an age-dependent increase in the AP and ML components in the TD group (R^2 = 0.4542 and 0.4154,
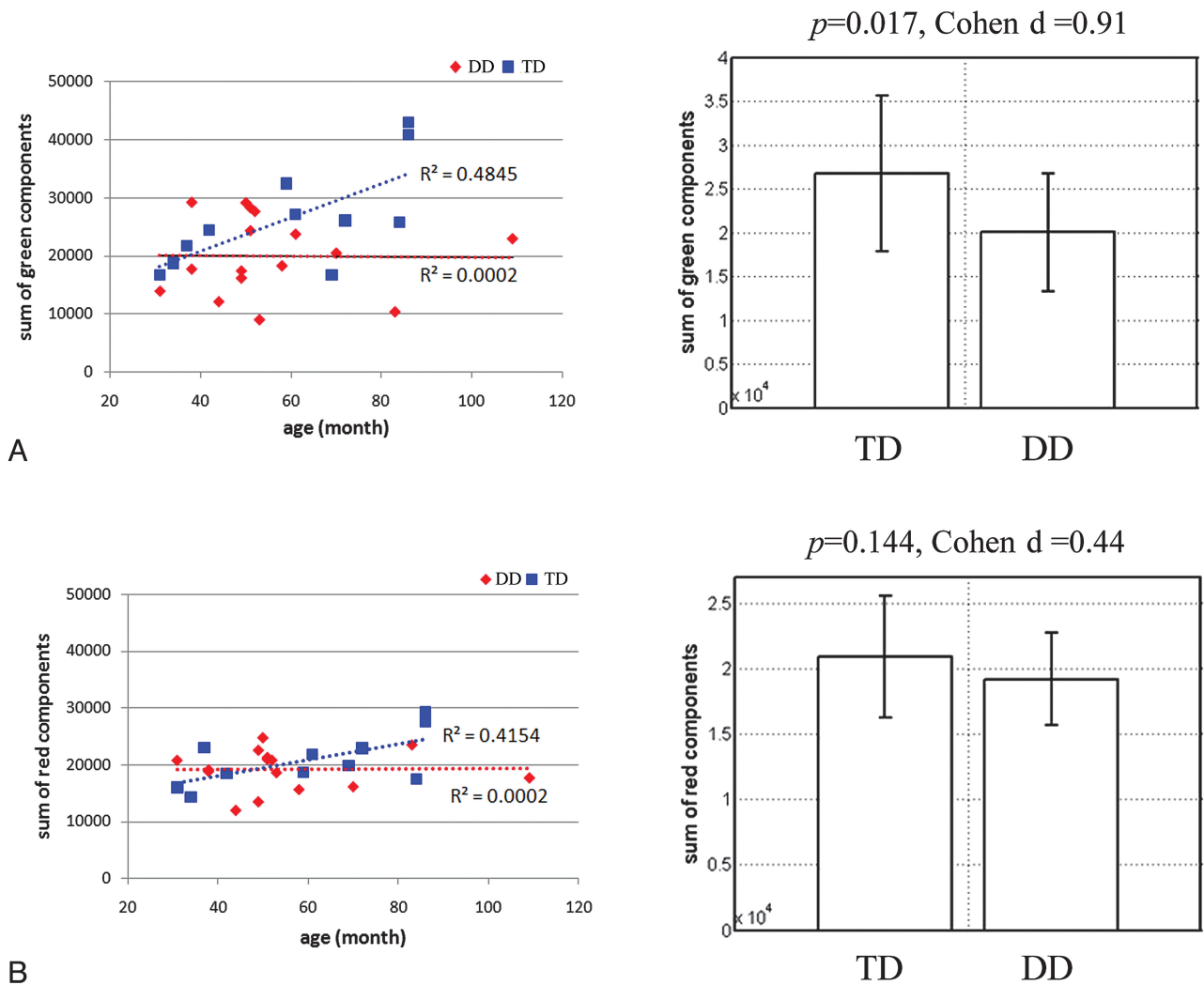
Fig 3. Results of region-based-quantification analysis. *A*, Sum of the AP component. *B*, Sum of the ML component. For both groups, 2 metrics are correlated with the age of the individual subject in terms of the linear regression coefficient, R^2 (left plot). The group mean and 1 SD of both metrics are displayed in the right plot.

respectively). However, we could not identify an age-dependent increase in both components in the DD group ($R^2 = 0.0002$ and 0.0002, respectively). The AP component was significantly decreased in the DD group (P value = .017 and effect size [Cohen d] = 0.91). Meanwhile the decrease of the ML component was not significant ($P = .144$ and effect size [Cohen d] = 0.44 for the ML component). Also to access the reliability of this analysis, 5 experienced neuroradiologists demarcated separate regions of interest in the MNI space. The interdrawer reliability was tested by calculating the Pearson correlation of the AP and ML components obtained from different drawers. The average and SD of correlation coefficients were 0.94 (0.05) and 0.87 (0.15) for the AP and ML components, respectively.

DTI Metric along the Entire AF Tract Bundle

The mean and SD of the FA, MD, AD, RD, and curvature along all the fiber bundles of both groups were measured before the TBM analysis. The FA was significantly lower in the DD group (0.37 ± 0.06 for TD and 0.31 ± 0.05 for DD, $P = .02$). Meanwhile other diffusivity parameters were higher in the DD group (MD: $7.95 \pm 0.77 \times 10^{-4}$ mm/s² for TD and

$8.68 \pm 0.14 \times 10^{-4}$ mm/s² for DD; AD: $11 \pm 0.91 \times 10^{-4}$ mm/s² for TD and $12 \pm 2.10 \times 10^{-4}$ mm/s² for DD; RD: $6.31 \pm 0.84 \times 10^{-4}$ mm/s² for TD and $7.22 \pm 1.15 \times 10^{-4}$ mm/s² for DD), consistent with those in our previous study.[23] Similar curvature was observed in both groups (0.07 ± 0.03 for TD and 0.07 ± 0.04 for DD). Only RD showed a significant increase in the DD group ($P = .05$). No significant differences were found in MD, AD, and curvature obtained from the entire tract ($P = .15$ for MD, $P = .61$ for AD, $P = 1$ for curvature).

TBM Analysis

The results of all TBM analyses along the TD prototype of the left AF group bundle are presented in Fig 4. For each arc-length coordinate of the TD prototype, each subject's mean of the DTI parameters was computed from all fibers belonging to the group bundle. The group mean and SD of the individual subject's means were plotted against arc-length coordinates in millimeters (left column of Fig 4). The statistical group differences in FA, MD, AD, RD, and curvature are shown in the middle and right columns (middle column for TD > DD and right column for TD < DD). The color bar indicates the FDR-
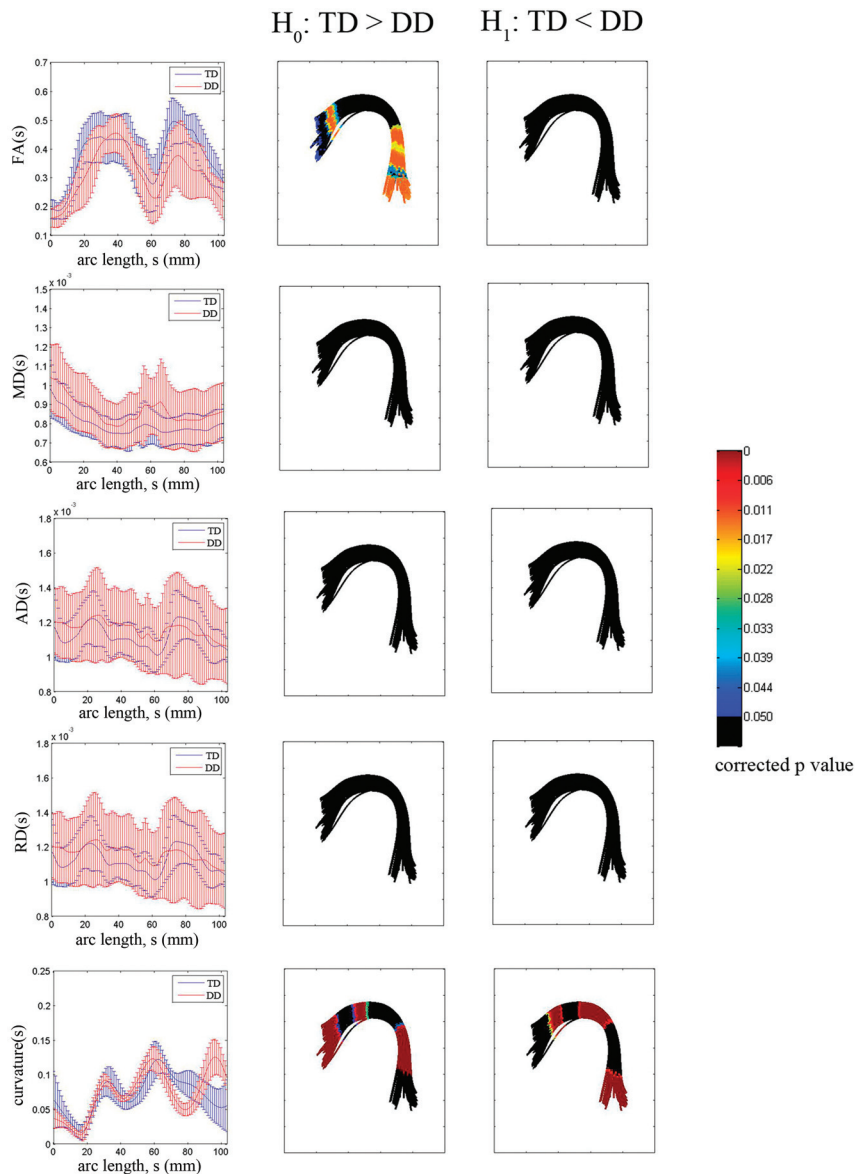
Fig 4. TBM group analysis of the left AF bundle by using a TD prototype fiber. For each arc-length coordinate (in millimeters), each subject's mean FA, MD, AD, RD, and curvature values are computed for the left AF bundle. The group mean and SD of these per-subject means are shown versus arc-length (left column). The multiple-comparison corrected *P* value for a significant difference on H_0 (TD > DD) or H_1 (TD < DD) is overlaid on corresponding segments of the DD group bundle (middle and right columns).

corrected *P* values. The multiple comparison FDR-corrected *P* value was color-coded on the surface of the DD group fiber bundle. Note that black is used to indicate the locations showing no significant group difference between the 2 groups (corrected *P* value < .05).

Compared with the group difference obtained from full-path analysis, the TBM analysis identified focal regions showing a significant difference even after correction for multiple comparisons. There was significantly decreased FA in 2 specific regions of the left AF—Broca area in the frontal lobe and Wernicke area in the temporal lobe (see TBM image in the middle of the first row). No significant difference was found in MD, AD, or RD at all arc-length coordinates (second, third, and fourth rows of Fig 4). The curvature TBM analysis captured a large amount of the shape variation between the 2 groups. Figure 4 (fifth row) shows that this variation is not

concentrated in 1 specific region but at multiple segments. The TD group showed higher curvatures in both language areas. The DD group produced higher curvatures in the region connecting both language areas (left parietal). The Table lists the MNI coordinates showing significant curvature differences in both groups.

The sensitivity of overall TBM results to the selection of the prototype was studied by defining common coordinates on the prototype fiber of the DD group and repeating the same TBM analysis as we did for Fig 4. We observed a very similar localization in all cases, indicating that the obtained TBM localization was independent of the selection of the prototype.

Discussion

This study found regional changes in FA and curvature of the left AF in children with DD, particularly involving the left

Table: MNI coordinates of fiber regions showing significant group difference in curvature[a]

Group	Curvature (mean ± SD)	MNI Coordinate (mm)		
		x	y	z
TD	0.0720 (0.0150)	−35.84	−31.95	27.86
DD	0.0932 (0.0142)			
TD	0.0565 (0.0247)	−49.68	−49.84	−2.19
DD	0.1247 (0.0258)			
TD	0.0808 (0.0165)	−41.76	−11.11	25.54
DD	0.0874 (0.0107)			
TD	0.0538 (0.0305)	−58.46	4.53	11.87
DD	0.0341 (0.0111)			
TD	0.0882 (0.0171)	−39.27	−50.70	9.89
DD	0.0500 (0.0089)			

[a] Corrected P value < .001.

inferior frontal and middle temporal regions of the tract. In addition, the children with DD did not display the typical pattern of age-related maturity of AP and ML pathways passing through the left arcuate region. This lack of age-related maturity was particularly striking in the AP pathways that correspond to the left AF.

Characterization of AF Abnormality
As mentioned previously, the classic AF fibers were unidentifiable in a significant fraction of children with DD in our prior study.[2] The same finding was observed even more dramatically in children with Angelman syndrome in whom the AF was unidentifiable in 6 of 7 subjects and barely identifiable in the remaining subject.[3] These findings suggest the importance of normal development of the AF for speech/language development. The AF may not be identifiable in DTI studies due to several reasons: agenesis, excessive pruning, poor myelination, or an aberrant course of the AF due to regional abnormalities along the AF path resulting from genetic abnormalities in molecular pathways involved in axonal guidance or scarring from brain injury blocking axonal growth.

Agenesis of large WM pathways is well-known for the corpus callosum, and genetic abnormalities in midline patterning, birth, and specification of commissural neurons and axon guidance have all been implicated in callosal agenesis.[24] Genetic abnormalities of axon-guidance pathways are major mechanisms underlying the abnormal development of WM tracts. Even though there are no animal/human studies that demonstrate the abnormalities in the axon-guidance mechanisms of the AF, specific axon guidance molecules that control the development of other tracts such as the corticospinal tract,[25] midbrain dopaminergic axons,[26] sensory axons,[27] olfactory pathway,[28] and ocular pathway[29] are increasingly being identified. While the degree of specificity of axon-guidance molecules that control WM development is not fully known, involvement of specific molecules such as *Semaphorin-6A*[25] (corticospinal tract), *fzd3/fzd6*[26] (midbrain dopaminergic axons), *Cadherin* Wernicke area [27] (sensory axons), the *Wnt* family of proteins[28] (olfactory pathway), and *Fzd5*[29] (ocular pathway) identified in these studies suggests that relatively specific mechanisms control the development of different WM pathways. This finding suggests that specific molecular mechanisms may be operative that could also disrupt the normal development of the AF. Similarly, DTI studies in knock-

out mice that disrupt axon guidance molecules show the lack of development of major pathways.[30] For example, *Fz-3−/−* knockout mice studies show an absence or severe reduction in the size of major axon tracts in the developing forebrain and a failure of sensory axons in the spinal cord to grow rostrally after crossing the midline.[30]

Similarly, any abnormality in the neurons at the origin or termination of the AF could result in the abnormal development of this tract. A microarray study to evaluate perisylvian cortical patterning identified several genes that are differentially expressed (25 upregulated and 147 downregulated) in the superior temporal gyrus relative to whole cerebral cortex.[31] Most of the upregulated genes encode transcription factors, while the downregulated genes were predominantly involved in neurite outgrowth and axon path finding. This study further confirmed the importance of axon-guidance abnormalities in the proper development of the perisylvian pathways such as the AF. Most interesting, this study also revealed that *CNTNAP2* was consistently expressed at higher levels in the middle and inferior frontal cortex compared with other cortical regions. The *CNTNAP2* gene is implicated in autism spectrum disorder[32,33] and is regulated by *FOXP2*.[34] An autosomal dominant mutation in the *FOXP2* gene has been found to be associated with developmental verbal dyspraxia during the investigation of 3 generations of the KE family.[35] Thus, abnormalities in the larger gene-regulation network in which *FOXP2-CNTNAP2* interaction occurs may be a common mechanism behind language disorders.[33] While the entire genetic network responsible for language and AF development has not yet been fully determined, these studies demonstrate key individual components of the network and their interaction patterns. Further studies to identify the determinants of unidentifiable AF will clarify this issue.

Methodologic Issues and Limitations
Most DTI-VBM analyses for the identification of regional abnormality in WM have been implemented by using sophisticated spatial normalization. An important strength of the proposed TBM analysis is that it performs tractwise statistical comparisons based on tract normalization across subjects (not based on scalar map normalization). In the present study, tract normalization was secured in 2 different aspects: 1) Whole-brain tractography of individual subjects was spatially registered across subjects by aligning brain maps to those of the template (SPM-DARETL normalization), and 2) normalized tracts of interest were reregistered across subjects by aligning them to the prototype.

We presume that these 2-step registrations yield a more efficient way to identify subtle group differences by performing statistical comparisons at anatomically equivalent locations across the subjects or groups. Although the accuracy of the SPM-DARTEL was successfully validated in a recent region-of-interest–based VBM study,[36] this normalization cannot guarantee perfect registration of all the fiber bundles over whole brain. In fact, the deformation was quite accurate at deep WM structures such as major association tracts but was not as accurate in subcortical peripheral WM regions. To overcome this limitation, future studies will incorporate more sophisticated schemes of spatial normalization using atlas-landmark-based multichannel deformation algorithms. An-

other limitation of the present study is the lack of quantitative neuropsychological data along different developmental domains. This limits our ability to perform correlations between DTI variables and developmental status or outcomes.

The current TBM analysis could not overcome partial volume effects of multiple tissue composites and fiber-crossings at single voxels because it performs statistical analysis on the basis of group bundles that were obtained by deterministic tractography. FA and curvature measured by using this methodology are also affected by these 2 factors. Thus, it is possible that they may be affected by anatomic differences of both groups and also differences in nearby or crossing tracts. Nonetheless, the TBM analysis for patients with DD is truly valuable because it provides a unique tool that can identify specific regions of the AF fibers showing aberrant variations in geometry. This cannot be detected by full-path analysis or other VBM approaches.

Conclusions

The present study demonstrated decreased regional anisotropy and sharper curvature of the left AF in children with DD in the inferior frontal and middle temporal regions. Children with DD also do not show the typical age-related maturational changes of the left AF. These findings are likely to be due to regional abnormalities in the axonal integrity of the left AF, thus providing new insights into abnormal development of the left AF in children with DD.

References

1. Filippi CG, Lin DDM, Tsiouris AJ, et al. **Diffusion-tensor MR imaging in children with developmental delay: preliminary findings.** *Radiology* 2003;229:44–50
2. Sundaram S, Sivaswamy L, Makki M, et al. **Absence of arcuate fasciculus in children with global developmental delay of unknown etiology: a diffusion tensor imaging.** *J Pediatr* 2008;152:250–55
3. Wilson BJ, Sundaram SK, Hug AH, et al. **Abnormal language pathway in children with Angelman syndrome: a diffusion tensor imaging (DTI) study.** *Ann Neurol* 2009;66:S109–09
4. Yamamoto N, Tamada A, Murakami F. **Wiring of the brain by a range of guidance cues.** *Prog Neurobiol* 2002;68:393–407
5. O'Donnell LJ, Westin CF, Golby AJ. **Tract-based morphometry for white matter group analysis.** *Neuroimage* 2009;45:832–44
6. Smith SM, Jenkinson M, Johansen-Berg H, et al. **Tract-based spatial statistics: voxelwise analysis of multi-subject diffusion data.** *Neuroimage* 2006;31:1487–505
7. Lee JE, Bigler ED, Alexander AL, et al. **Diffusion tensor imaging of white matter in the superior temporal gyrus and temporal stem in autism.** *Neurosci Lett* 2007;7:127–32
8. Basser PJ, Mattielo J, Le Bihan D. **MR diffusion tensor spectrography and imaging.** *Biophys J* 1994;66:259–67
9. Basser PJ, Pierpaoli C. **Microstructural and physiological features of tissues elucidated by quantitative-diffusion-tensor MRI**. *J Magn Reson B* 1996;111:209–19
10. Batchelor PG, Calamante F, Tournier JD, et al. **Quantification of the shape of fiber tracts.** *Magn Res Med* 2006;55:894–903
11. Ashburner J. **A fast diffeomorphic image registration algorithm.** *Neuroimage* 2007;38:95–113. Epub 2007 Jul 18
12. Kelin J, Andersson BA, Ardekani J, et al. **Evaluation of 14 nonlinear deformation algorithms applied to human brain MRI registration.** *Neuroimage* 2009;46:786–802
13. Wilke M, Schmithorst VJ, Holland SK. **Assessment of spatial normalization of whole-brain magnetic resonance images in children.** *Hum Brain Mapp* 2002;17:48–60
14. Brun A, Park HJ, Knuttsson H, et al. **Coloring of DT-MRI fiber traces using Laplacian eigenmaps.** *In:* Diaz RM, Arencibia AQ (eds). *Computer Aided Systems Theory (EUROCAST '03), Lecture Notes in Computer Science 2809.* Las Palmas de Gran Canaria, Spain: Springer Verlag, 2003;564–72
15. Yuan W, Holland SK, Schmithorst VJ, et al. **Diffusion tensor MR imaging reveals persistent white matter alternation after traumatic brain injury experienced during early childhood.** *AJNR Am J Neuroradiol* 2007;28:1919–25
16. Alexander DC, Pierpaoli C, Basser PJ, et al. **Spatial transformations of diffusion tensor magnetic resonance images.** *IEEE Trans Med Imaging* 2001;20:1131–39
17. Xu D, Mori S, Shen D, et al. **Spatial normalization of diffusion tensor fields.** *Magn Reson Med* 2003;50:175–82
18. Zhang W, Li X, Zhang J, et al. **Landmark-reference voxel-based analysis of diffusion tensor images of the brain stem white matter tracts application in patients with middle cerebral artery stroke.** *Neuroimage* 2009;44:906–13
19. Li H, Xu Z, Guo L, et al. **A hybrid approach to automatic clustering of white matter fibers.** *Neuroimage* 2010;49:1249–58
20. Ruiz-Alzola J, Westin CF, Warfield SK, et al. **Nonrigid registration of 3D scalar vector and tensor medical data.** *Med Image Anal* 2002;6:143–61
21. Tzourio-Mazoyer N, Landeau B, Papathanassiou D, et al. **Automated anatomical labeling of activations in SPM using a macroscopic anatomical parcellation of the MNI MRI single-subject brain.** *Neuroimage* 2002;15:273–89
22. Yekutieli D, Benjamini Y. **Resampling-based false discovery rate controlling multiple test procedure.** *J Statist Plann Inference* 1999;82:171–96
23. Kumar A, Sundaram SK, Sivaswamy L, et al. **Alternations in frontal lobe tracts and corpus callosum in young children with autism spectrum disorder.** *Cereb Cortex* 2010;20:2103–13. Epub 2009 Dec 17
24. Paul LK, Brown WS, Adolphs R, et al. **Agenesis of the corpus callosum: genetic, developmental and functional aspects of connectivity.** *Nat Rev Neurosci* 2007;8:287–99
25. Rüenker AE, Little GE, Suto F, et al. **Semaphorin-6A controls guidance of corticospinal tract axons at multiple choice points.** *Neural Dev* 2008;3:34
26. Stuebner S, Faus-Kessler T, Fischer T, et al. **Fzd3 and Fzd6 deficiency results in a severe midbrain morphogenesis defect.** *Dev Dyn* 2010;239:246–60
27. Steinel MC, Whitington PM. **The atypical cadherin Flamingo is required for sensory axon advance beyond intermediate target cells.** *Dev Biol* 2009;327:447–57. Epub 2008 Dec 30
28. Rodriguez-Gil DJ, Greer CA. **Wnt/Frizzled family members mediate olfactory sensory neuron axon extension.** *J Comp Neurol* 2008;511:301–17
29. Lie C, Nathans J. **An essential role for frizzled 5 in mammalian ocular development.** *Development* 2008;135:3567–76. Epub 2008 Oct 2
30. Wang Y, Zhang J, Mori S, et al. **Axonal growth and guidance defects in Frizzled3 knock-out mice: a comparison of diffusion tensor magnetic resonance imaging, neurofilament staining, and genetically directed cell labeling.** *J Neurosci.* 2006;26:355–64
31. Abrahams BS, Tentler D, Perederiy JV, et al. **Genome-wide analyses of human perisylvian cerebral cortical patterning.** *Proc Natl Acad Sci U S A* 2007;104:17849–54. Epub 2007 Oct 31
32. Alarcón M, Abrahams BS, Stone JL, et al. **Linkage, association, and gene-expression analyses identify CNTNAP2 as an autism-susceptibility gene.** *Am J Hum Genet* 2008;82:150–59
33. Poot M, Beyer V, Schwaab I, et al. **Disruption of CNTNAP2 and additional structural genome changes in a boy with speech delay and autism spectrum disorder.** *Neurogenetics* 2010;11:81–89
34. Vernes SC, Newbury DF, Abrahams BS, et al. **A functional genetic link between distinct developmental language disorders.** *N Engl J Med* 2008;359:2337–45
35. Vargha-Khadem F, Gadian DG, Copp A, et al. **FOXP2 and the neuroanatomy of speech and language.** *Nat Rev Neurosci* 2005;6:131–38
36. Bergouignan L, Chupin M, Czechowska Y, et al. **Can voxel-based morphometry, manual segmentation and automated segmentation equally detect hippocampal volume differences in acute depression.** *Neuroimage* 2009;45:29–37